metals

MDPI

Article

Effect of Hot Mill Scale on Hydrogen Embrittlement of High Strength Steels for Pre-Stressed Concrete Structures

Marina Cabrini [1,2,3,*], Sergio Lorenzi [1,2,3], Tommaso Pastore [1,2,3] and Diego Pesenti Bucella [1,2]

1 Department of Engineering and Applied Sciences, University of Bergamo, Dalmine (BG) 24044, Italy; sergio.lorenzi@unibg.it (S.L.); tommaso.pastore@unibg.it (T.P.); diego.pesentibucella@unibg.it (D.P.B)
2 Consorzio Superfici Grandi Interfase (CSGI), Unit of Research of Bergamo, Dalmine (BG) 24044, Italy
3 Consorzio Interuniversitario Nazionale per la Scienze e Tecnologia dei Materiali (INSTM), Unity of Research of Bergamo, Dalmine (BG) 24044, Italy
* Correspondence: marina.cabrini@unibg.it; Tel.: +39-035-2052-318

Received: 2 February 2018; Accepted: 23 February 2018; Published: 3 March 2018

Abstract: The presence of a conductive layers of hot-formed oxide on the surface of bars for pre or post-compressing structures can promote localized attacks as a function of pH. The aggressive local environment in the occluded cells inside localized attacks has as consequence the possibility of initiation of stress corrosion cracking. In this paper, the stress corrosion cracking behavior of high strength steels proposed for tendons was studied by means of Constant Load (CL) tests and Slow Strain Rate (SSR) tests. Critical ranges of pH for cracking were verified. The promoting role of localized attack was confirmed. Further, electrochemical tests were performed on bars in as received surface conditions, in order to evaluate pitting initiation. The adverse effect of mill scale was recognized.

Keywords: stress corrosion cracking; localized corrosion; pre-stressed concrete; hydrogen embrittlement

1. Introduction

Due to the high stress involved, bars made of high strength alloys are preferentially used as short tendons for post-tensioning. In fact, they are very susceptible to small damages, such as surface scratches, corrosion cracks and pits, which usually do not affect the performance of bars for concrete reinforcement [1]. Stress corrosion cracking is one the most probable causes of failure of high strength tendons in pre-stressed or post-stressed concrete structures [2–5]. These corrosion phenomena occur in the form of cracks, which nucleate and propagate due to combined action of tensile stresses and aggressive environment. Failures can take place at stress lower than yield strength of the steel, with catastrophic consequences on the structures stability and for people safety [1,6,7].

Susceptibility to stress corrosion cracking increases with tensile strength of materials and occurs above a threshold stress value. The more load increases above this critical limit, the more time to rupture decreases [8,9]. Since high strength steels, stressed to very high load (up to 80% of tensile yield strength), are utilized for tendons, critical conditions for stress corrosion cracking can be reached.

Susceptibility depends on composition, microstructures, and mechanical properties of the steels [10–12].

The older pre-stressed concrete structures were realized using quenched and tempered steels with high susceptibility to EAC [13,14]. Later, cold drawn eutectoid steels were widely used in pre-stressed concrete structures [15,16]. Moreover, it depends on environmental parameters, such as dissolved salt

in water, pH and potential. The presence of conductive layers on the surface can promote localized attacks, with formation of local environment in the occluded cells [17], critic for the initiation of stress corrosion cracking [3,18].

In concrete structures, bars can be exposed to different environments, because these are used as external or internal unbonded tendons or bonded tendons embedded in concrete. The pH of solutions is usually alkaline (concrete pore solutions and bleeding waters), but neutral or acid values can be found, due to humidity condensation and atmospheric water penetration in ungrouted ducts. The composition depends on rainwater, atmospheric pollution (SO_2), distance from the sea (Cl^-) and soluble salts that can be washed away by water percolation on structure.

Literature data explain the SCC of high strength steels through a mechanism based on hydrogen embrittlement. Nürberger [19] reported on a statistical study of failures due to SCC and pointed out the effect of the localized corrosion for achieving critical ranges of potential and pH. However, there is lack of experimental data about the effects of environmental parameters. Furthermore, the SCC susceptibility of steels is normally evaluated by means of standard tests, as FIP thiocyanate test, which is quite different from field conditions.

Aim of the research is to evaluate the behaviour to SCC of commercial bars for pre-stressed concrete structures. The paper reports the results of the tests performed in order to study the critical ranges of pH for the initiation of stress corrosion cracking and the effect on localized attack of surface conditions of the bars.

2. Materials and Methods

The chemical composition and mechanical properties of the steels are reported in Table 1. The bars were produced through an in-line heat treatment by water quenching with self-tempering. Thus, a different microstructure between core and surface layers is observed. The external layer is characterized by tempered martensite, with hardness in the ranges 390–410 $HV_{200,15}$ and 360–380 $HV_{200,15}$ for the two steels respectively (Figure 1). The bars are covered by a mill scale.

Table 1. Chemical composition and mechanical properties of the considered steels.

Steel	Chemical Composition (% Weight)					Mechanical Properties	
	C	Mn	Si	P	S	R_S (MPa)	R (MPa)
A	0.71	0.63	0.22	0.016	0.016	996	1103
B	0.2	1.45	0.45	0.022	0.017	713	818

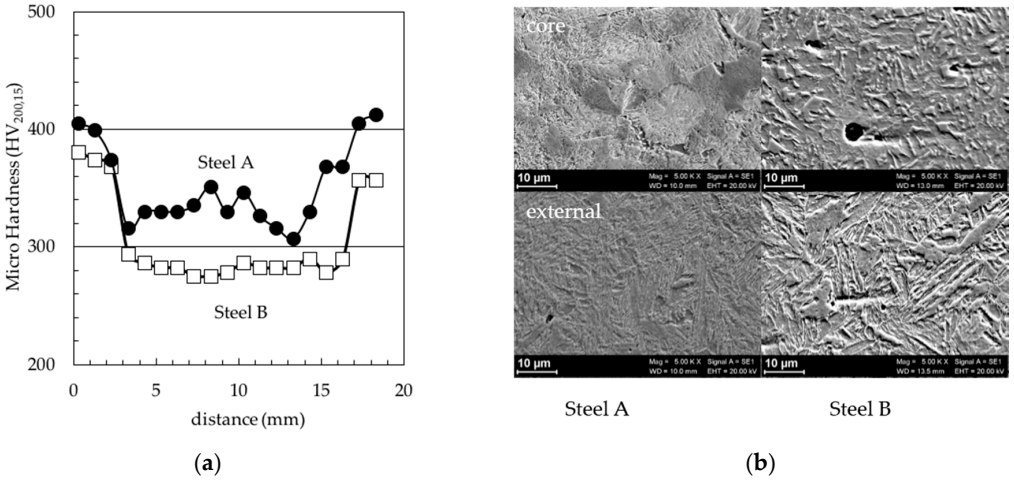

Figure 1. (**a**) Vickers 200g micro-hardness profile ($HV_{200,15}$) and (**b**) microstructure (5000×) of the considered steels.

Constant Load tests and Slow Strain Rate (SSR) tests were performed on 3 mm diameter cylindrical tensile specimens. Since the different microstructures between core and surface of the bars, the specimens were machined from a high strength martensitic steel with microstructure and hardness (400 $HV_{200,15}$) similar to that of the surface layer. The tests were performed in aerated hydrochloric acid solutions with pH from 3 to 6.4, at the free corrosion potential. Some tests were also executed in de-aerated solutions. Constant Load tests were carried out at 90% of yield strength.

SSR tests were performed according to ISO 7539-7 at 10^{-6} s^{-1} strain rate. SCC was evaluated through the reduction in area ratio (i.e., ratio between the value of area reduction after test in solution and the value of area reduction after the test in air) and the presence of brittle areas on fracture surface and secondary cracks.

The electrochemical tests were performed on specimens cut from bars of steel A and steel B, with as received surfaces—covered by the mill scale—and after pickling by inhibited hydrochloric acid. Monitoring of free corrosion potential and polarization resistance of bars during 1 month immersion test, Cathodic and Anodic Polarization Potentiodynamic (PD) and Cyclic Voltammetry tests (CV) were carried out.

Solutions of Portland cement, calcium and sodium hydroxide were used as test environments at pH between 9 and 14. Dilute hydrochloric acid solutions were utilized for more acid solutions (5.5 to 7 pH). The specimens were covered by epoxy resin in order to leave only the lateral surface exposed at the aggressive environments. Corrosion potential was monitored by means of a data recording. Linear Polarization Resistance (LPR) was measured through a potentiodynamic method, in the range of $\pm$10 mV vs E_{corr} at 10 mV/min scan rate.

Potentiodynamic tests were carried out with a scan rate of 0.166 mV/s on rotating electrode at 2500 rpm; cathodic potentiodynamic curves were started from the corrosion potential and finished at $-$1.5 V vs SCE; anodic cyclic potentiodynamic tests were started from $-$0.2 V vs E_{corr} with a vertex potential of +1.5 V vs SCE.

Cyclic voltammetry tests were performed after 15 s of equilibration at open circuit potential (OCP) for two consecutive voltammetry cycles, from $-$1.7 to +0.7 V vs. SCE at 50 mV/s scan rate.

All the tests were twice conducted and a good reproducibility was detected.

3. Results and Discussion

Stress Corrosion Tests

Stress corrosion cracking of high strength steels takes place with a hydrogen embrittlement mechanism. Atomic hydrogen produced from the cathodic reduction of hydrogen ions is adsorbed on the metal surface, diffuses into the metal lattice and can promote the insurgence of cracks in the presence of a tensile stress. The cracks grow under the synergic action of stress and environment until the final mechanical failure is reached [20,21].

Hydrogen ions reduction is the main cathodic reaction in acid environments; in neutral or alkaline media it could take place only under cathodic polarization at very negative potentials, which can be reached only in the presence of cathodic protection systems or galvanic coupling with less noble metals [22,23].

Stress corrosion cracking insurgence increases in acid environments at pH lower than 5. Figure 2 illustrates the environmental effect on the tensile stress-strain curve of the steels during SSR tests. The curves drawn during tests in solution with pH above 4 showed no appreciable differences with respect to the curves obtained in air. Both in aerated and de-aerated solutions with pH below 5, low ductility is found. Such loss in ductility is induced by clear brittle cracking on the fracture surface (Figure 3a). In solutions with pH 3, secondary transgranular cracks, perpendicular to the applied stress, were found (Figure 3b). At higher pH, secondary cracks also grew along slip plane on a 45° direction, in areas very close to the fracture surface of specimens heavily strained, producing the characteristic aspect described (Figure 3b). Thus, the embrittlement phenomena become more pronounced as pH

decreases (Figure 4). The loss in ductility due to environment is expressed in Figure 5a as reduction of area ratio (ratio between the value of the reduction of area in environment and the reduction of area in air — R.A.%environment/R.A.%air). Low values of this parameter indicate the insurgence of SCC phenomena.

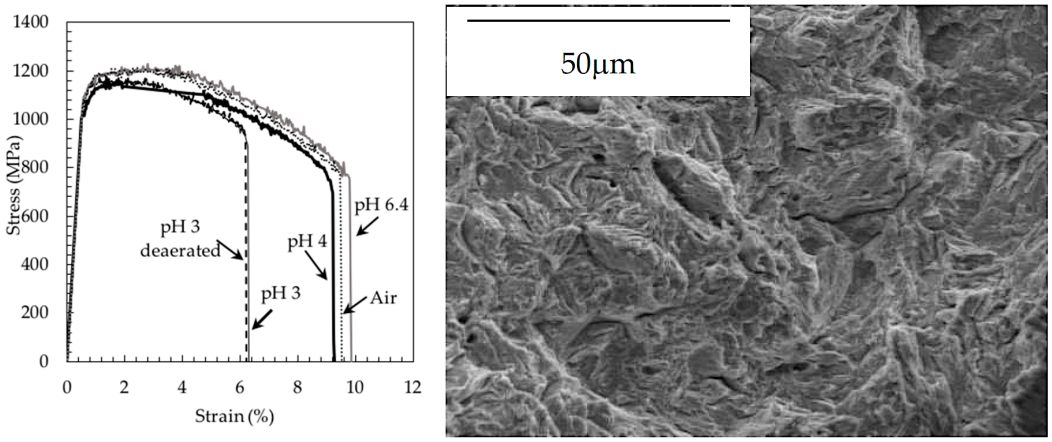

Figure 2. (**a**) Effect of pH solution on the tensile loading curve during SSR tests; (**b**) Fracture surface of the specimen after the SSR test at pH 3 in de-aerated solution (1000×).

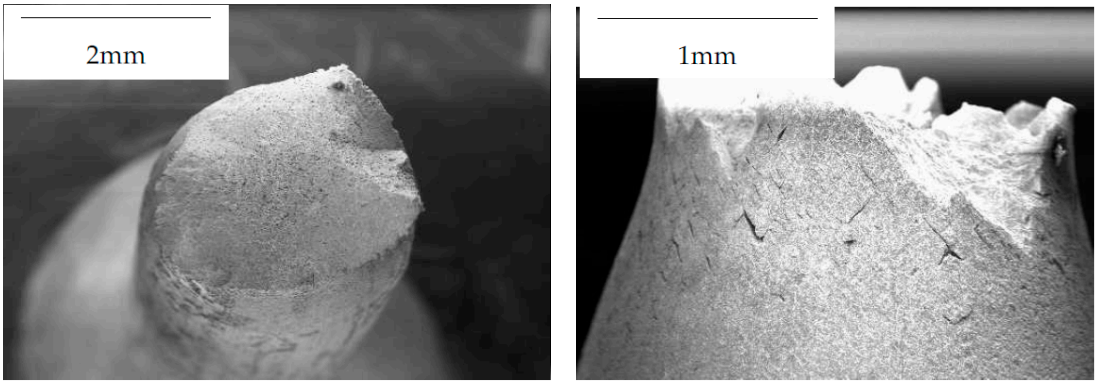

Figure 3. (**a**) Fracture surface of the specimen after the SSR test at pH 3 in aerated solution (50×); (**b**) Growth along slip plane of secondary cracks on the specimens after the SSR test at pH 4.

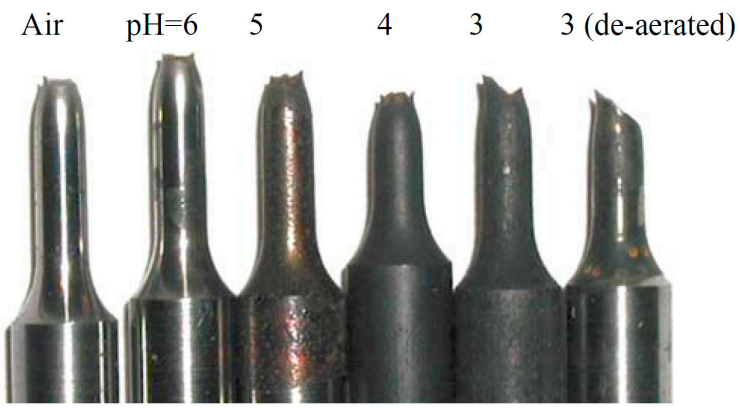

Figure 4. Effect of pH on the fracture morphology of the specimens.

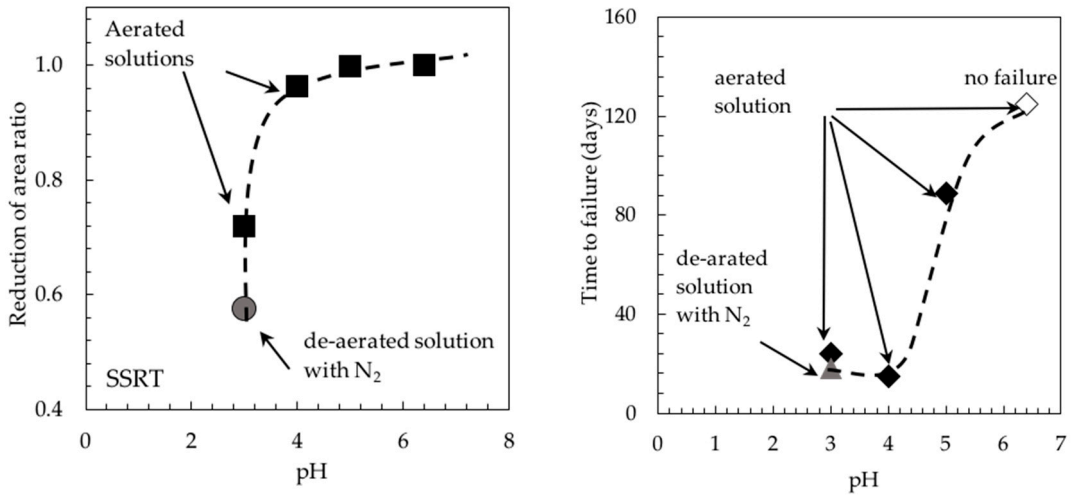

Figure 5. Effect of pH on (**a**) the area ratio (R.A.%environment/R.A.%air); (**b**) the time to failure of the Constant Load test specimens.

The results of Constant Load tests confirm the effect of pH on SCC. Figure 5b shows the time to failure of specimens loaded at 90% of yield strength. The time to failure increases with pH; specimens did not break in the solution with pH 6 after 4 months of testing.

The critical range for SCC is quite lower than the pH of the solutions usually found in the structures. Bonded tendons are usually grouted with alkaline mortar, with pH higher than 12.5. However, the metal surface can be wetted by less alkaline solutions before grouting, or in incompletely grouted ducts and in unbonded tendons without any protection system (such as coating) applied on metal surfaces. Bleeding waters show pH between 9 and 12. Very low pH (below 5) can only be measured in rainwater and condensations in areas with high pollution [24–26].

However, Constant Load tests even showed well detectable SCC phenomena at pH 5 after long time testing. The cracks initiated from localized attack, as shown in Figure 6.

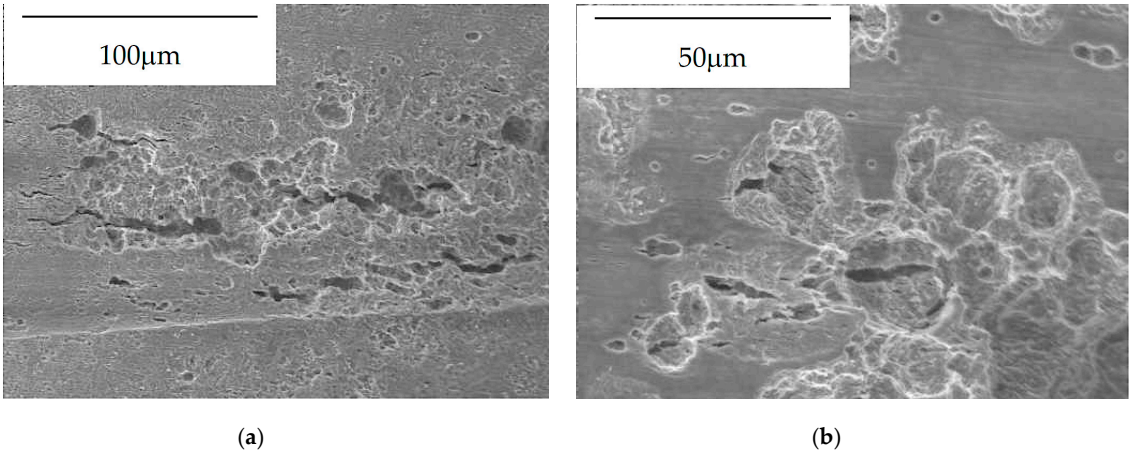

Figure 6. (**a**) Secondary cracks initiated from pit after Constant Load test in solution with pH 4. (**b**) close-up of (**a**) at higher magnification.

Inside the occluded cell, formed by the localized attack, the pH sensibly decreases and can reach values below 4 due to hydrolysis of metal ions. Consequently, the critical range of pH can be reached, promoting stress corrosion initiation. This mechanism was proposed by Nürberger in order to explain

the failure of pre-stressing steels observed in neutral and alkaline solutions. The specimen failure takes place after a time needed to form the occluded cell [19,27].

Localized attacks can occur in alkaline environments with pH above 11.5, in the presence of a sufficient concentration of chloride that can break down the passive film on steel. This case may occur in concrete exposed to chloride-containing environment, due to the penetration of these ions until the bar surface. In neutral-alkaline environments, carbon steel is not passive. The main cause of localized attacks is the presence of a mill scale (mainly calamine), formed on the steel surface during hot rolling. The corrosion rate of carbon steel can be enhanced by galvanic coupling with calamine, which is an electronic conductive oxide, inducing localized corrosion on the anodic areas not covered by the scale. The galvanic coupling considerably increases the corrosion potential of the steel (Figure 7) during the initial period. Specimens in as received surface conditions showed a corrosion potential 100–250 mV nobler than the specimens after pickling, when they are just immersed in the test solution. Moreover, the difference tends to increase over time in all the considered solutions. Such an anodic polarization induces very high corrosion rate on the anodic areas.

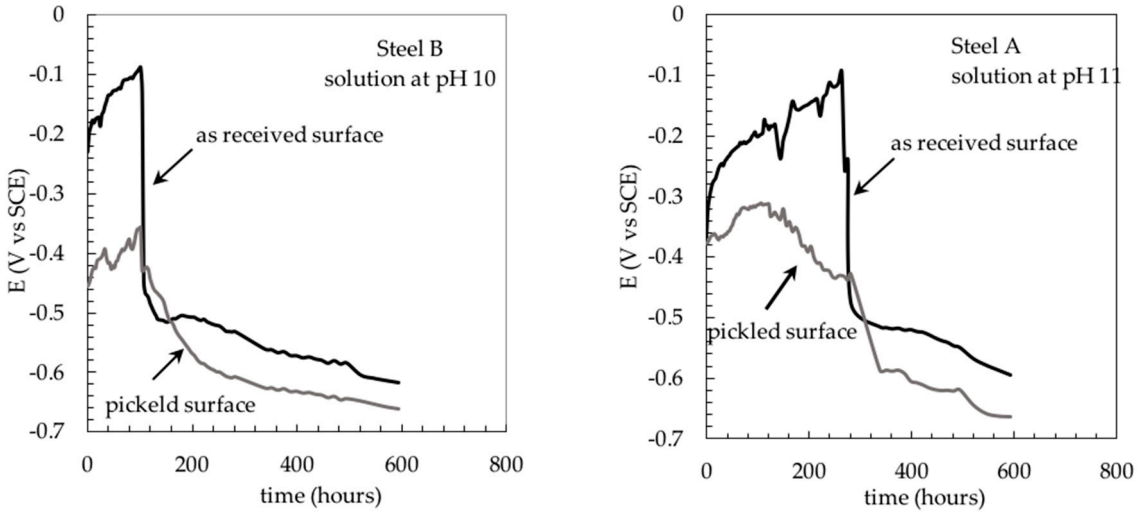

(**a**) (**b**)

Figure 7. Corrosion potential vs time curves for the tested steels in solution at (**a**) pH 10 and (**b**) pH 11.

After the initial period, depending on the pH of the solution, the anodic polarization due to calamine becomes no more significant. The corrosion potential decreases to active potentials of pickled specimens due to the formation of deep localized attacks and the progressive change of the oxide scale, which is not stable at room temperature (Figure 7). Thus, the effect of calamine is especially evident in the first periods of exposure, which is a function of pH, increasing with it.

Figure 8 compares the polarization resistances measured on the specimens in as received surface conditions with mill scale and after pickling. The average corrosion rate evaluated on the specimens in as received conditions is initially low (high values of the polarization resistance in Figure 8) because of very small anodic areas uncovered by the scale. Afterwards, the corrosion rate of the specimens tends to similar values of pickled specimens.

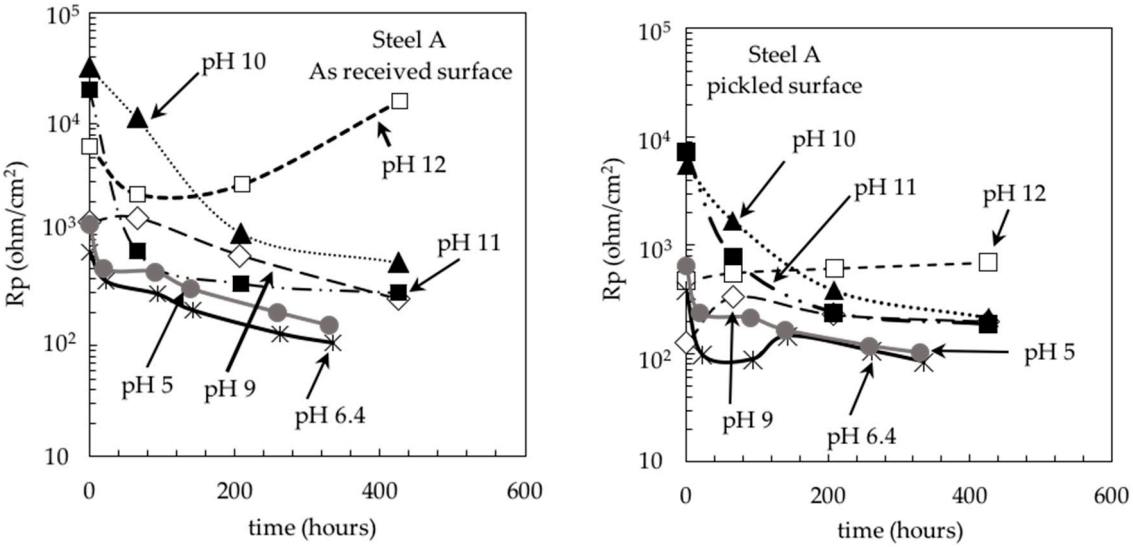

Figure 8. Polarization resistance vs time curves for steel A, as a function of different pH, with (**a**) as received surface and (**b**) pickled surface.

Figure 9 shows the specimens after the immersion tests at different pH. At pH lower than 10 and higher than 12, there are no differences between the specimens with as received or pickled surface. In the first case, a generalized corrosion was observed, whereas at pH higher than 12 all the specimens are in passive conditions, without evidence of corrosion products. In the range of pH from 10 and 11, the pickled specimens showed uniform corrosion; on the contrary, the specimens with as received surface showed un-attacked areas, with the presence of calamine and some corroded regions around the un-attacked areas. No differences between the two considered steels were founded in the electrochemical behavior.

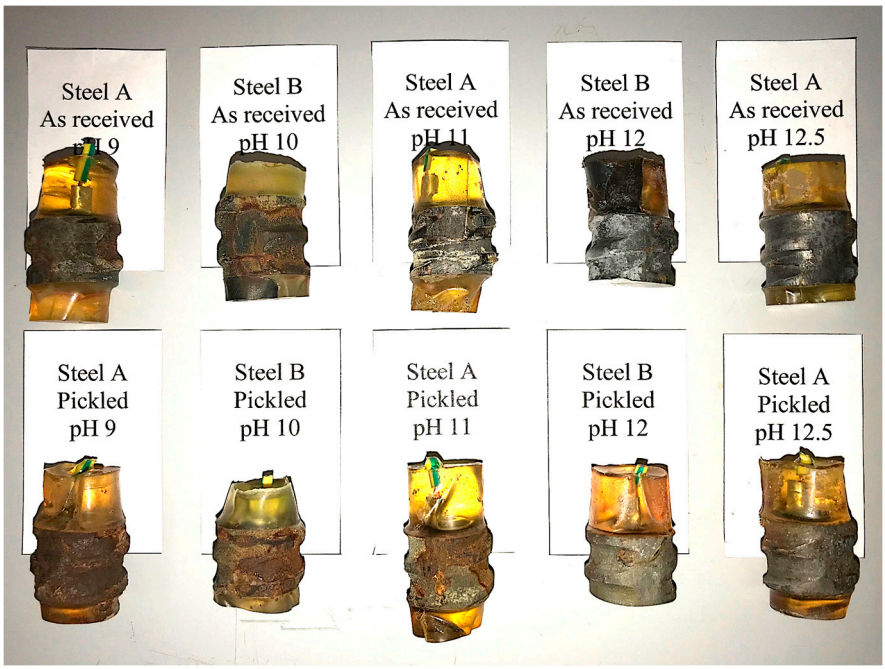

Figure 9. Specimens with as received or pickled surface after the immersion tests at different pH.

Figure 10a shows the potentiodynamic cathodic curves obtained on as received surface and after pickling. The pickled surface was also tested after 48 h of passivation in the solution. It could be noted that the specimens with presence of calamine have low overvoltages at potentials above the oxygen limiting current density zone. The data confirm that calamine can act as a good cathode for the oxygen reduction.

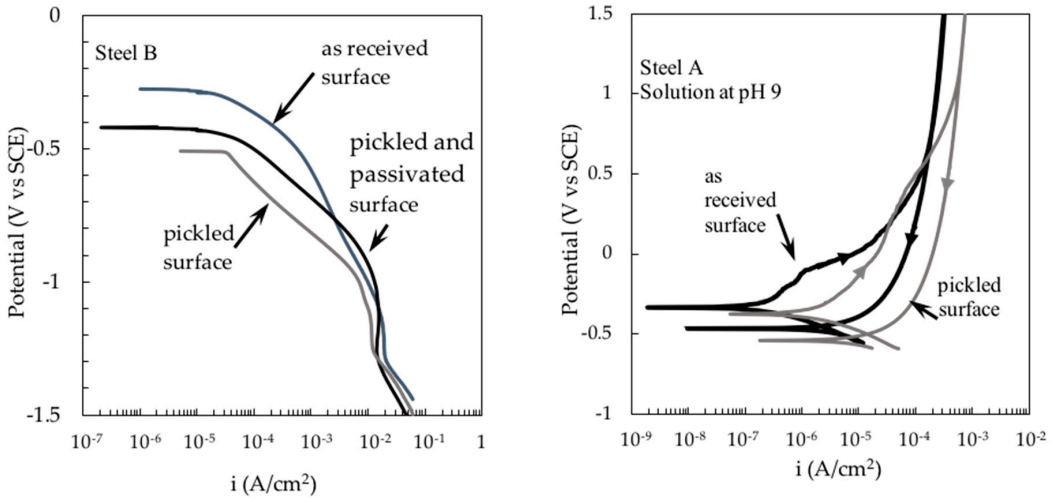

(**a**) (**b**)

Figure 10. Effect of surface conditions on (**a**) cathodic potentiodynamic curves of the steel B in alkaline solution (pH 14) and (**b**) anodic cyclic potentiodynamic curves of the steel A in pH 9 solution.

Figure 10b and Figure 11 show the effect of mill scale on the cyclic potentiodynamic curves as a function of pH. The mill scale modifies the anodic polarization curves of the steels. In solution at pH less than 11, the steels show active dissolution, independently from the surface conditions (Figure 10b). At pH 13, a passive behavior was always observed (Figure 11a). In the pH range between 11 and 13 it is possible to observe noticeable differences between the anodic cyclic potentiodynamic curves.

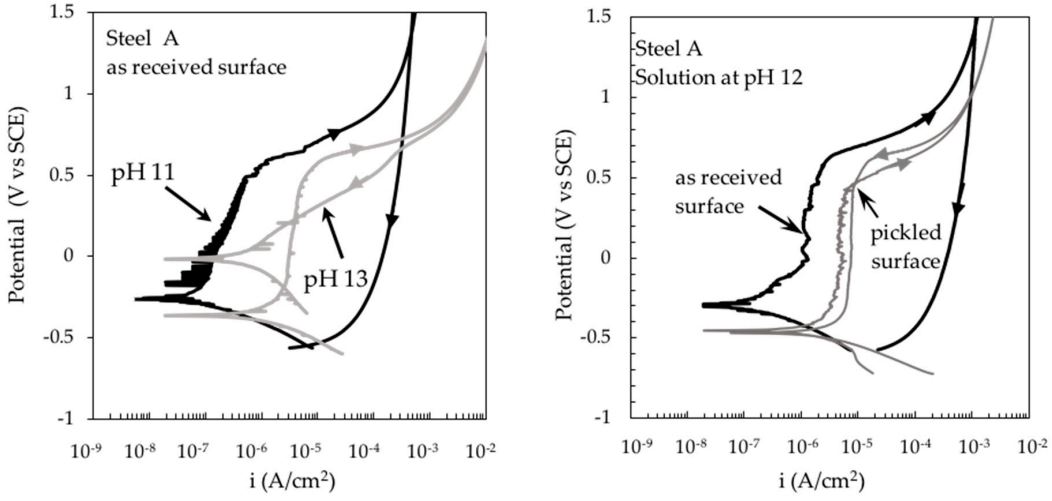

(**a**) (**b**)

Figure 11. (**a**) Effect of pH on anodic cyclic potentiodynamic curves of the steel A in as received conditions, covered by a mill scale; (**b**) Effect of surface conditions on anodic cyclic potentiodynamic curves of the steel A in pH 12 solution.

The anodic current is low for the as received surface specimen at the beginning of the test, due to the presence of the oxide scale that protects the metal surface. Oxygen evolution at high potentials, both on steel and on scale, produces similar current densities on as received specimens and pickled specimens. After the potential scan is inverted, the specimens with as received surface show a great hysteresis, while the specimens with polished surface maintain a passive behavior (Figure 11b).

The calamine oxide scale can stimulate the localized corrosion of the steel in all the situations characterized by the absence of grouting with alkaline mortar or corrosion protection systems that prevent the direct contact between the steel and the solution. In alkaline mortar, the steel becomes passive and shows potentials similar to those of the calamine. Thus, no galvanic couple takes place. In solution with pH below 11.5, which is the limit of pH for the passivity of the steel in solutions without chlorides, the galvanic effect of calamine can be considerable. This behavior is well illustrated by the potentiodynamic curves of Figure 11, in which the pickled surface did not show hysteresis during the reverse of potential; instead, the hysteresis is very evident on the as received surfaces.

In the cyclic voltammetry tests (Figure 12) it is possible to observe the appearance of the passivation peaks of the iron only at pH 12.5. At pH 12, a hint of peaks appears, more pronounced for specimens with pickled surface than those with as received surface. The current values recorded for the pickled specimens are higher than those for specimens with the as received surface, shielded from the calamine scale. Once the passivation of the specimen intervenes, the cathodic reduction of oxygen on as received specimens occurs at a potential lower than the values observed on pickled specimens, confirming the electrocatalytic effect of the calamine. With respect to literature data [28–30], the peak of the Fe/Fe(II) reaction is not present on the cyclic voltammetric curve, for all the surface conditions of the specimens. This could be due to the presence of the hot-formed oxide on the specimens, but it also shows how pickling cannot restore an iron surface completely absent from oxides. On the other hand, the presence for all the specimens of the large oxidation peak from Fe(II) to Fe(III) clearly indicates that the hot-formed oxide film does not isolate the underlying metal from the environment. On the contrary, it allows the irreversible growth of the film by anodic oxidation, as shown by the increase in the amplitude of the peak in the second potential cycle and by the absence of the conjugate reduction peak.

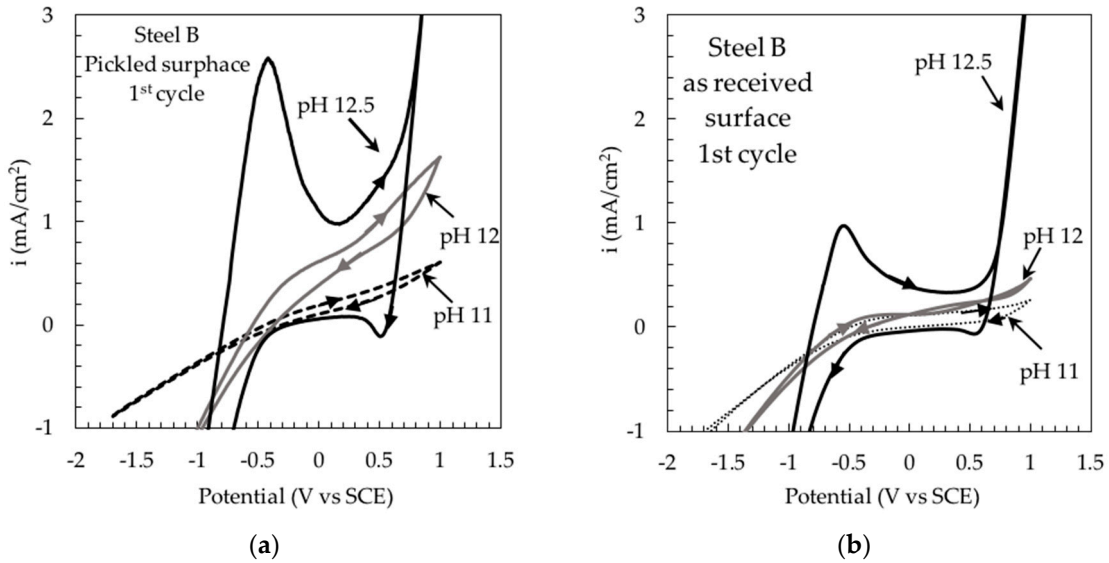

Figure 12. Cyclic voltammetry tests of steel B in solution at different pH; (**a**) specimens with pickled surface; (**b**) specimens with as received surface.

From these tests, it is possible to hypothesize that the film present on the bars with as received surface is not stable in solution, but tends to dissolve with pH greater than 12.5–13, it has a good

electrical and ionic conductivity and allows the oxidation of the underlying metal and, finally, it has a low overvoltage for oxygen.

It is therefore conceivable that, in case of partial covering of the surface with this oxide, which occurs as the oxide tends to melt, there may be localized corrosion between the areas still covered with oxide and those with non-coated surfaces. This can be done for all pH investigated up to 12.5: beyond this value, the specimen can passivate. At pH < 12 there is a competition between the location of the attack between shielded areas and free areas, and the dissolution of the oxide film. The lower the pH of the solution, the greater the speed of destruction of the film, so it is conceivable that the maximum localization of the attack is for pH between 11 and 12. These results are confirmed by the observation of the samples recovered after the monitoring of the corrosion potential at different pH (Figure 7).

Finally, the promoting role of calamine on stress corrosion cracking in neutral or slight alkaline solutions can be sketched as proposed in Figure 13.

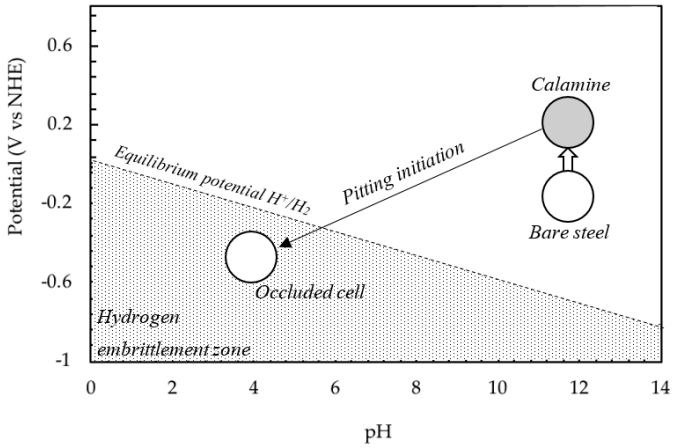

Figure 13. Role of calamine on insurgence of favorable conditions for hydrogen embrittlement in neutral or slight alkaline environment.

When a bar is embedded in alkaline solutions at pH higher than 12.5, this becomes passive, independently from the surface conditions. If the pH of the environment decreases at values lower than 12, the presence of calamine increases the corrosion potential of the bar and, in the area where the oxide scale is not present, some localized attacks may be initiated. Inside the localized attack, the pH decreases and, contemporaneously, the open circuit potential decreases too, so the hydrogen evolution reaction becomes possible. In these conditions, in the presence of susceptible steel and mechanical stress, hydrogen embrittlement can take place. For very high strength steels, with a low critical intensity factor, very small defect generated by hydrogen embrittlement can promote brittle catastrophic fracture [1].

4. Conclusions

The paper studies the condition for initiation of localized attacks on high strength steel for post-tensioning structures as a function of superficial conditions. SCC tests were performed on a martensitic steel with the same hardness compared to that obtained in peripheral zones of hot worked and quenched bars. Stress corrosion can occur in solutions with pH below 5 due to hydrogen embrittlement. The pH inside the localized attacks reaches values lower than 5 owing to the well knows mechanism of the occluded cell. In the absence of chlorides, the initiation of localized attacks occurs due to the presence of oxide scale produced by hot-working and the pH of the environment. Localized attacks initiate in a critical range of pH between 10 and 12. At pH higher than 12.5, the bar is passive independently upon the surface conditions. pH values lower than 10 promote the occurrence

of general corrosion. At pH values lower than 12, the presence of calamine increases the corrosion potential of the bar and localized attacks can occur in the zones not protected by the oxide layer.

Hydrogen embrittlement can produce very small defects, which can promote brittle fracture in high strength steels characterized by low fracture toughness. The results pointed out the negative effect played by the mill scale for applications in which the reinforcements are protected by mortars characterized by low alkalinity, mainly below pH values of 12.

Author Contributions: Pastore and Cabrini conceived and designed the experiments; Pesenti Bucella performed the experiments, photographed the specimens, reviewed the English form; Lorenzi analyzed the data. All the authors contributed to write the paper.

Conflicts of Interest: The authors declare no conflict of interest.

References

1. Valient, A.; Elices, M. Premature failure of prestressed steel bars. *Fail. Anal. Case Stud. II* **1998**, *5*, 219–227. [CrossRef]
2. Monfore, G.; Verbeck, C. Corrosion of prestressed wire in concrete. *J. Am. Concr. Inst.* **1960**, *37*, 491–516.
3. Perrin, M.; Gaillet, L.; Tessier, C.; Idrissi, H. Hydrogen embrittlement of prestressing cables. *Corros. Sci.* **2010**, *52*, 1915–1926. [CrossRef]
4. Yuyama, S.; Yokoyama, K.; Niitani, K.; Ohtsu, M.; Uomoto, T. Detection and evaluation of failures in high-strength tendon of prestressed concrete bridges by acoustic emission. *Constr. Build. Mater.* **2007**, *21*, 491–500. [CrossRef]
5. Stoll, F.; Saliba, J.; Casper, L. Experimental study of CFRP-prestressed high-strength concrete bridge beams. *Compos. Struct.* **2000**, *49*, 191–200. [CrossRef]
6. Woodward, R.; Williams, F. Collapse of Ynys-y-Gwas Bridge, west Glamorgan. *Proc. Instn. Civ. Engrs.* **1988**, *84*, 635–669. [CrossRef]
7. Helmerich, R.; Zunkel, A. Partial collapse of the Berlin Congress Hall on May 21st 1980. *Eng. Failure Anal.* **2014**, *43*, 107–119. [CrossRef]
8. Senigaglia, D.; Re, G.; Pedeferri, P. *Cedimento per Fatica e Ambientale dei Materiali Metallici*; CLUP: Milano, Italy, 1979.
9. Pedeferri, P.; Bertolini, L. *La Durabilità del Calcestruzzo Armato*; Mc Graw-Hill: Milano, Italy, 2000; p. 199.
10. Woodtli, J.; Kieselbach, R. Damage due to hydrogen embrittlement and stress corrosion cracking. *Eng. Failure Anal.* **2000**, *7*, 427–450. [CrossRef]
11. Cabrini, M.; Lorenzi, S.; Marcassoli, P.; Pastore, T. Hydrogen embrittlement behavior of HSLA line pipe steel under cathodic protection. *Corros. Rev.* **2011**, *29*, 261–270. [CrossRef]
12. Cabrini, M.; Lorenzi, S.; Pellegrini, S.; Pastore, T. Environmentally assisted cracking and hydrogen diffusion in traditional and high-strength pipeline steels. *Corros. Rev.* **2015**, *33*, 529–545. [CrossRef]
13. Mietz, J. Investigation on hydrogen-induced embrittlement of quenched and tempered prestressing steels. *Mater. Corros.* **2000**, *51*, 2–80. [CrossRef]
14. Darmawan, M.; Stewart, M. Effect of pitting corrosion on capacity of prestressing wires. *Mag. Concr. Res.* **2007**, *59*, 131–139. [CrossRef]
15. Toribio, J.; Ovejero, E. Effect of Cold Drawing on Microstructure and Corrosion Performance of High-Strength Steel. *Mech. Time-Depend. Mater.* **1998**, *1*, 307–319. [CrossRef]
16. Enos, D.; Scully, J. A Critical-Strain Criterion for Hydrogen Embrittlement of Cold-Drawn, Ultrafine Pearlitic Steel. *Metall. Mater. Trans. A* **2002**, *33A*, 1151–1166. [CrossRef]
17. Zitrou, E.; Nikolaou, J.; Tsakiridis, P.; Papadimitriou, G. Atmospheric corrosion of steel reinforcing bars produced by various manufacturing processes. *Constr. Build. Mater.* **2007**, *21*, 1161–1169. [CrossRef]
18. Vehovar, L.; Kuhar, K.; Vehovar, A. Hydrogen-assisted stress corrosion of prestressing wires in a motorway viaduct. *Eng. Failure Anal.* **1998**, *5*, 21–27. [CrossRef]
19. Nürnberger, U. *Korrosion und Korrosionsschutz im Bauwesen*; Grundlagen, B., Metallbau, K., Eds.; Bauverlag BV GmbH: Gütersloh, Germany, 1995.
20. Hirth, J. Effects of Hydrogen on the Properties of Iron and Steel. *Metall. Trans. A* **1980**, *11A*, 861–890. [CrossRef]

21. Lynch, S. Hydrogen embrittlement phenomena and mechanisms. *Corros. Rev.* **2012**, *30*, 105–123. [CrossRef]
22. Bockris, J.O.; McBreen, J.; Nanis, L. The Hydrogen Evolution Kinetics and Hydrogen Entry into a-Iron. *J. Appl. Electrochem.* **1965**, *112*, 1025–1031. [CrossRef]
23. Cabrini, M.; Lorenzi, S. Pipeline Steels: Hydrogen Diffusion and Environmentally Assisted Cracking. In *Encyclopedia of Iron, Steel, and Their Alloys*; George, E., Totten, R.C., Eds.; CRC Press Taylor and Francis Group: Boca Raton, FL, USA, 2016; pp. 2547–2599.
24. Camuffo, D.; Bernardi, A.; Zanetti, M. Analysis of the Real-Time Measurement of the oH of Rainfall at Padova, Italy: Seasonal Variatino and Meteorological Aspects. *Sci. Total. Environ.* **1988**, *71*, 187–200. [CrossRef]
25. Mrose, H. Measurements of pH, and chemical analyses of rain-, snow-, and fog-water. *Tellus* **1966**, *18*, 266–270. [CrossRef]
26. Singh, A.; Agrawal, M. Acid rain and its ecological consequences. *J. Environ. Biol.* **2008**, 15–24.
27. Nürnberger, U. Corrosion induced failure mechanisms of prestressing steel. *Mater. Corros.* **2002**, *53*, 591–601. [CrossRef]
28. Schrebler Guzmán, R.S.; Vilche, J.R.; Arvia, A.J. The potentiodynamic behaviour of iron in alkaline solutions. *Electrochim. Acta* **1979**, *24*, 395–403. [CrossRef]
29. Cabrini, M.; Lorenzi, S.; Pastore, T. Cyclic voltammetry evaluation of inhibitors for localised corrosion in alkaline solutions. *Electrochim. Acta* **2014**, *124*, 156–164. [CrossRef]
30. Schrebler Guzman, R.S.; Vilche, J.R.; Arvia, A.J. The voltammetric detection of intermediate electrochemical processes related to iron in alkaline aqueous solutions. *J. Appl. Electrochem.* **1981**, *11*, 5. [CrossRef]